Cascadia Subduction Earthquakes

Leonard et al 2010

Rupture area and displacement of past Cascadia great earthquakes from coastal coseismic subsidence

GSA Bulletin 122: 2079-2096

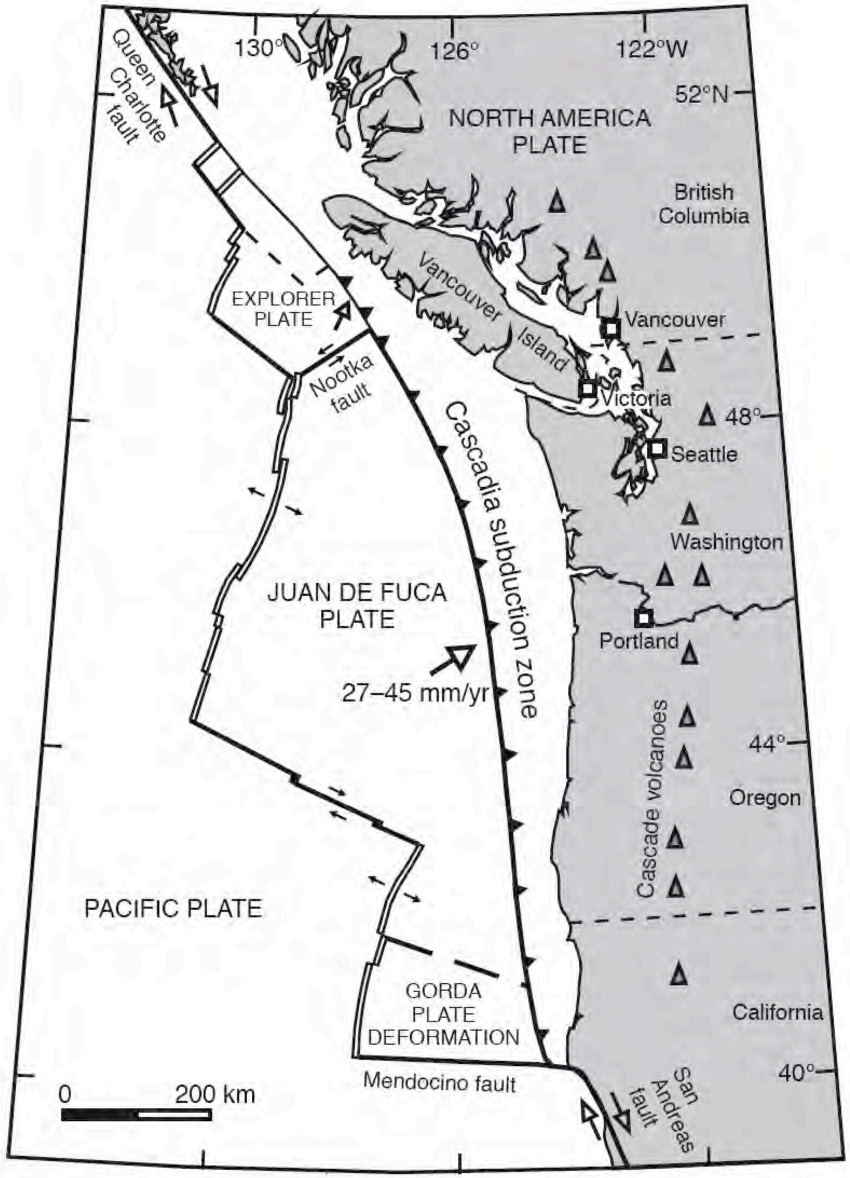

Figure 1. Plate-tectonic setting of the Cascadia subduction zone. The study covers the Juan de Fuca–North America plate boundary from the Mendocino fault in the south to the Nootka fault in the north. Tectonic deformation is complex at the southern and northern ends of the subduction zone. In this study, the Explorer plate subduction in the north is assumed to be independent.

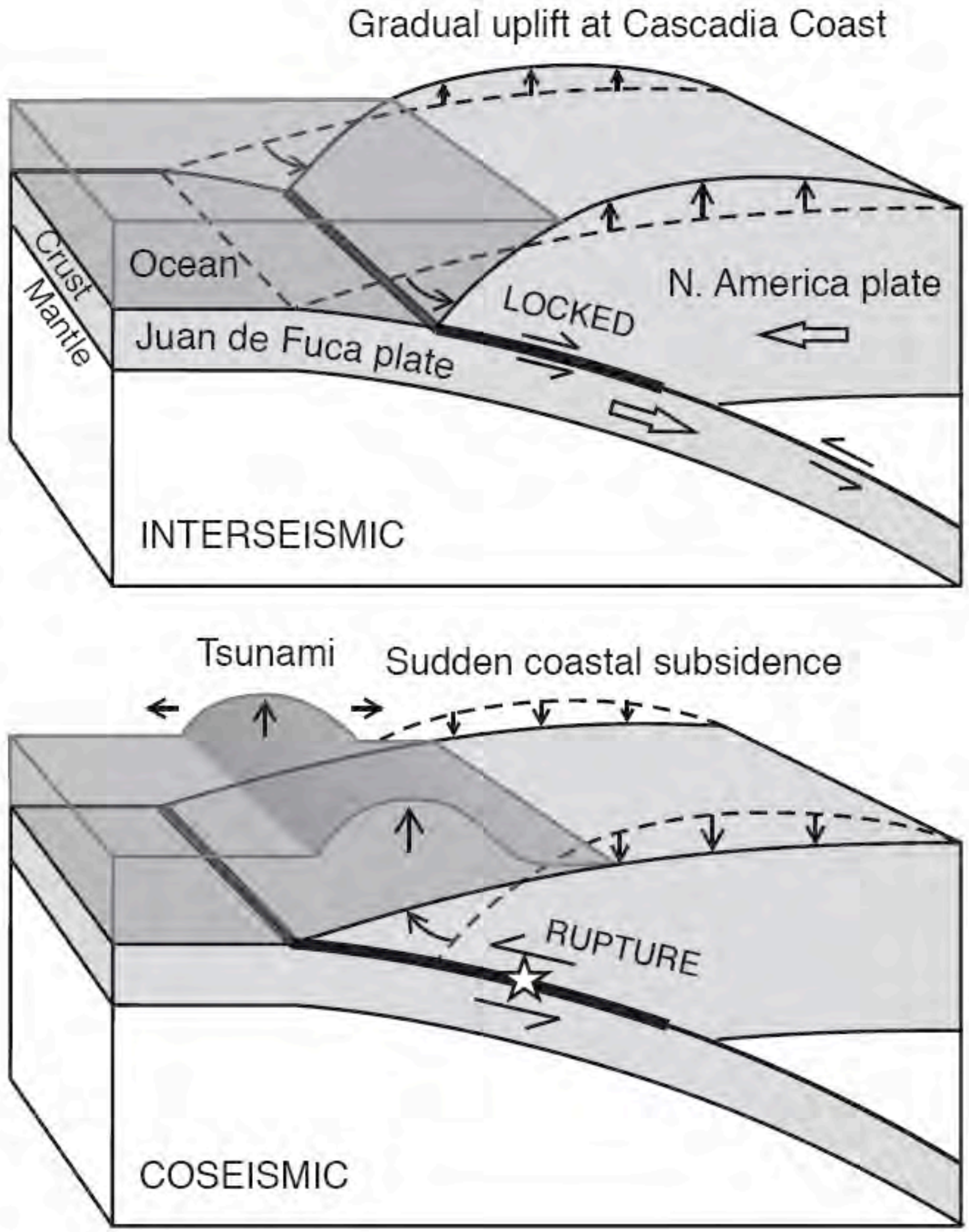

Figure 2. Pattern of interseismic and coseismic deformation associated with a subduction thrust fault (modified from Atwater et al., 2005). Note that the magnitude of uplift/subsidence varies with distance from the locked/rupture zone.

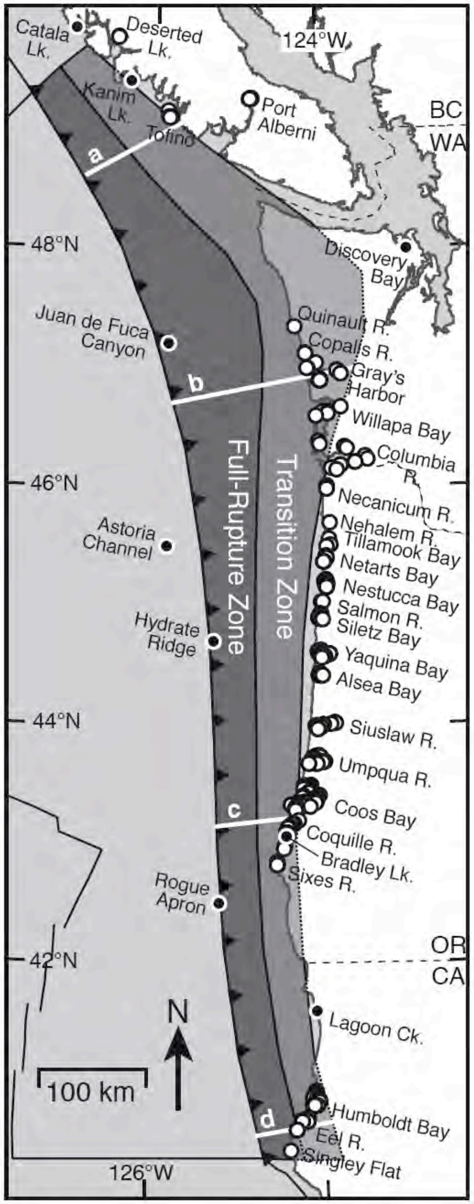

Figure 3. Location of coastal data sites relative to the full-rupture (dark gray) and transition (medium gray) zones. White-filled circles—buried soil sites. Black-filled circles—tsunami/turbidite deposit sites. White lines labeled a–d show locations of profiles in Figures 9 and 11.

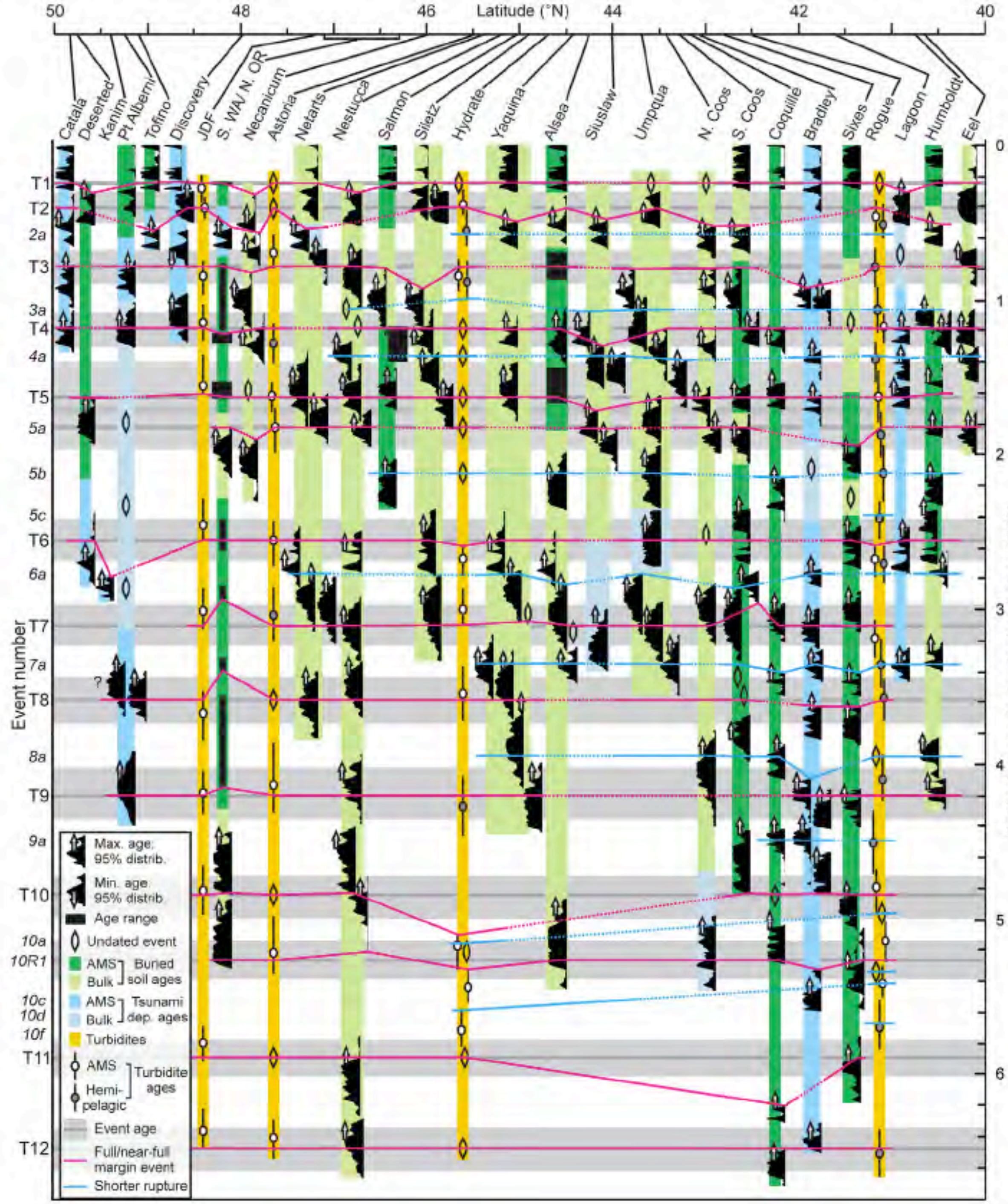

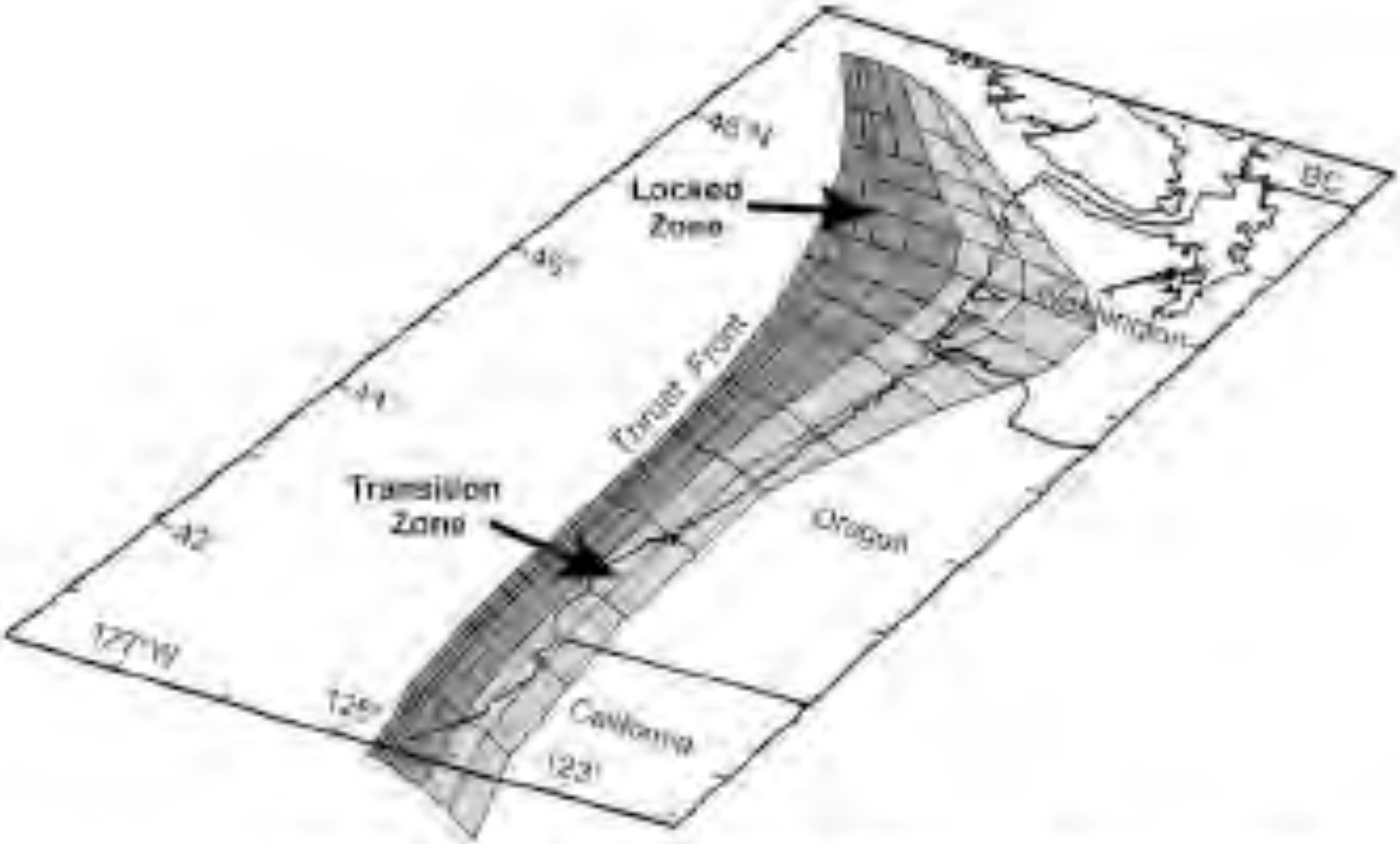

Figure 8. Locked and transition zones of Cascadia megathrust (based on thermal constraints and geodetic data) used in elastic dislocation model (after Flück et al., 1997).

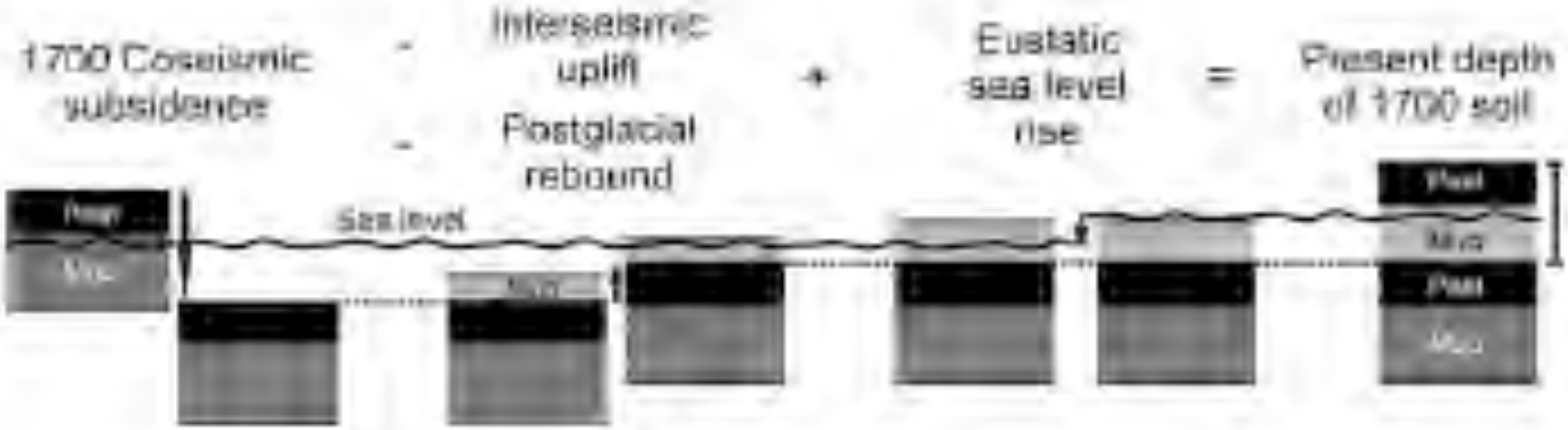

1700 Coseismic subsidence = Present depth of 1700 soil + Interseismic uplift + Postglacial rebound - Eustatic sea level rise

1700 Coseismic subsidence - Present depth of 1700 soil - Postglacial rebound + Eustatic sea level rise = Interseismic uplift since 1700

Figure 12. Method 2: Method for estimating coseismic subsidence using depth of 1700 peat horizon below modern marsh top (results in Fig. 13). Also shown is an independent method of estimating interseismic uplift since 1700, using marsh coseismic subsidence estimates, depth of 1700 horizon, postglacial rebound, and eustatic sea-level rise (results in Fig. 14).

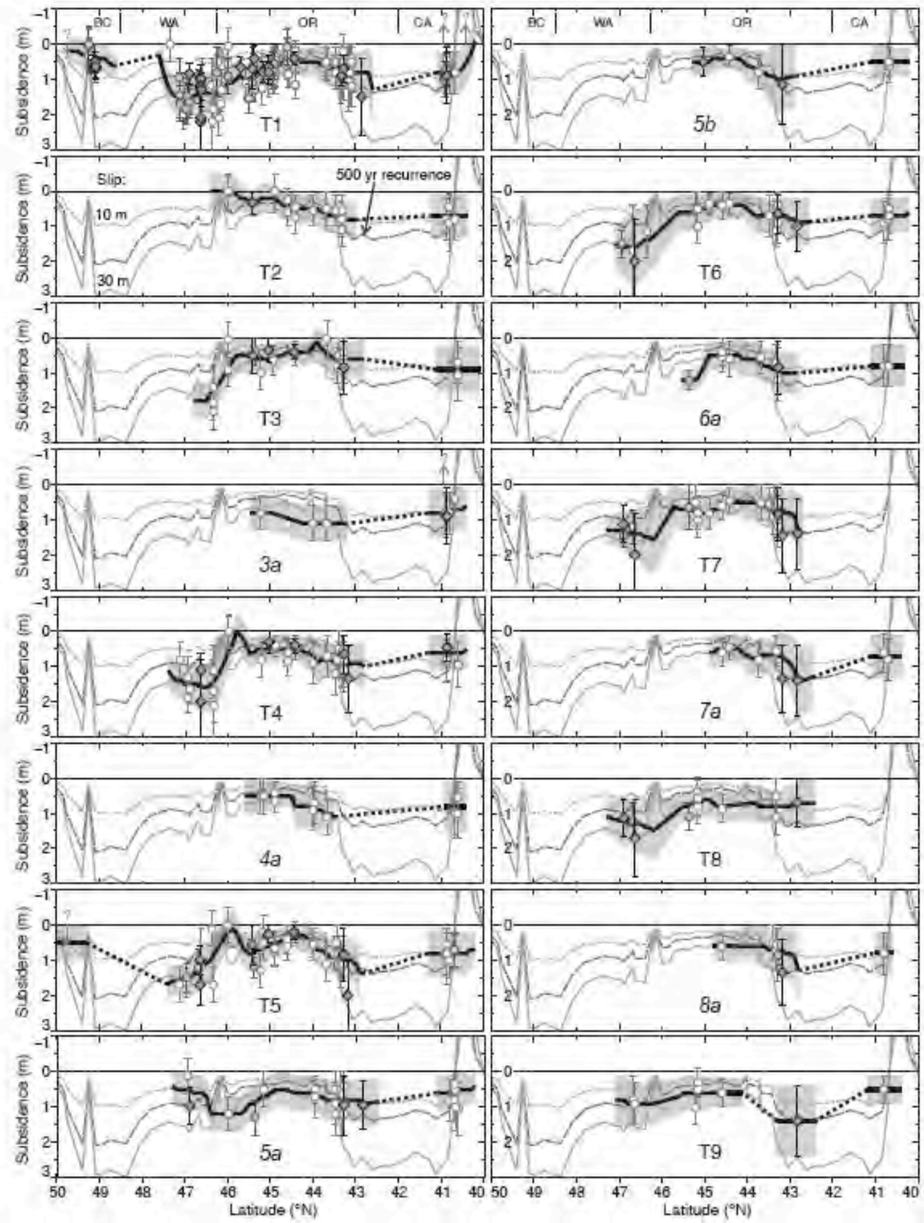

Figure 5. Estimated coseismic subsidence in events 1–9 (T1–T9), as correlated in Figure 4, plotted against latitude (data details in Table DR1 [see footnote 1]). Gray diamonds represent high-quality estimates from statistical microfossil analyses; gray circles are medium-quality estimates from relative organic content, with macrofossil data on both sides of the contact and/or relative fresh/brackish diatom concentration; white circles are low-quality estimates from relative organic content, with macrofossil data for one/no sides of the contact. Thick black lines and gray shading represent the weighted average (moving average over 1°) and uncertainty, respectively, of estimated coseismic subsidence. Upward/downward arrows with question marks indicate unquantifiable estimates of uplift/subsidence. Thinner lines (labeled for event 2) show the predicted subsidence for megathrust slip of 10 m and 30 m (light-gray lines) and for the release of 500 yr of accumulated strain (dark-gray dashed line). See Table 1 for data sources.

Figure 6. Comparison of coseismic subsidence and megathrust slip among the A.D. 1700 earthquake (T1), previous recorded events (averaged), and the predictions of elastic dislocation models. Subsidence and slip estimate details are given in Table 1 (with all subsidence data in Table DR1 [see footnote 1]). (A) Averaged locations of coastal coseismic subsidence sites relative to the full-rupture (purple) and transition (lilac) zones. White diamonds and circles—sites with high- and low-quality subsidence estimates, respectively. See Figure 3 for site names. White arrows—plate convergence vectors. (B) Coseismic subsidence estimated at the above buried soil sites for the A.D. 1700 earthquake (red symbols and shading—weighted mean and uncertainty) and for pre–A.D. 1700 recorded events (blue symbols and shading—mean and uncertainty). Upward/downward arrows with question marks indicate unquantifiable estimates of uplift/subsidence. Two low-quality data points are excluded from the shading as they appear to be outliers; these include data from the Columbia River that are questionable due to possible freshwater influence (Leonard et al., 2004). Dashed dark-gray lines show coseismic subsidence predicted by the elastic dislocation model at the same sites for the release of 200 and 500 yr of accumulated strain. (C) As in B, except the gray lines represent coseismic subsidence predicted for uniform megathrust slip of 10, 20, and 30 m. (D) Along-strike megathrust slip variations estimated for the A.D. 1700 (red symbols and shading—weighted mean and uncertainty) and previous events (blue symbols and shading—mean and uncertainty) from the correspondence between observed coseismic subsidence and that predicted from uniform slip models (C). Dark-gray lines show the along-margin slip pattern expected for the release of 200, 500, and 1000 yr of accumulated strain.

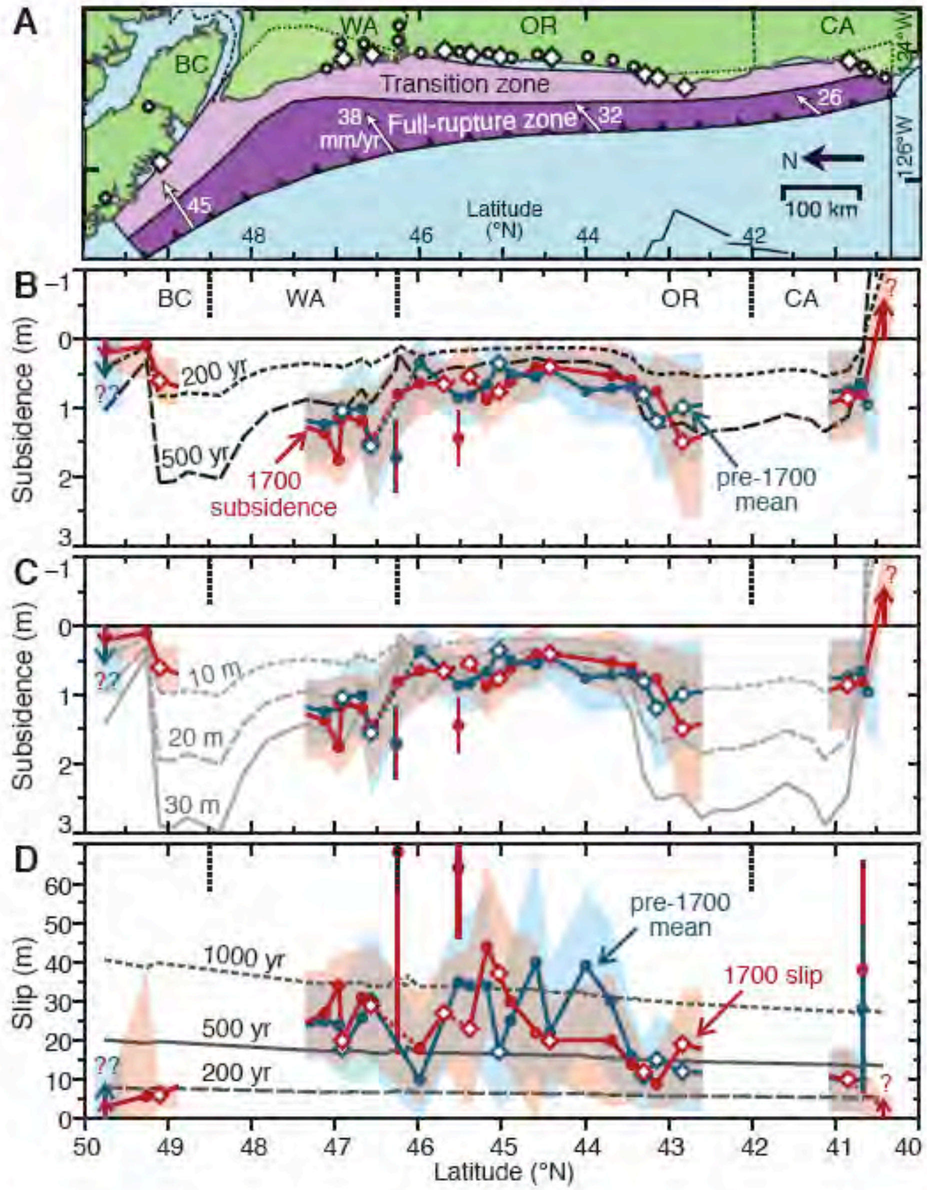

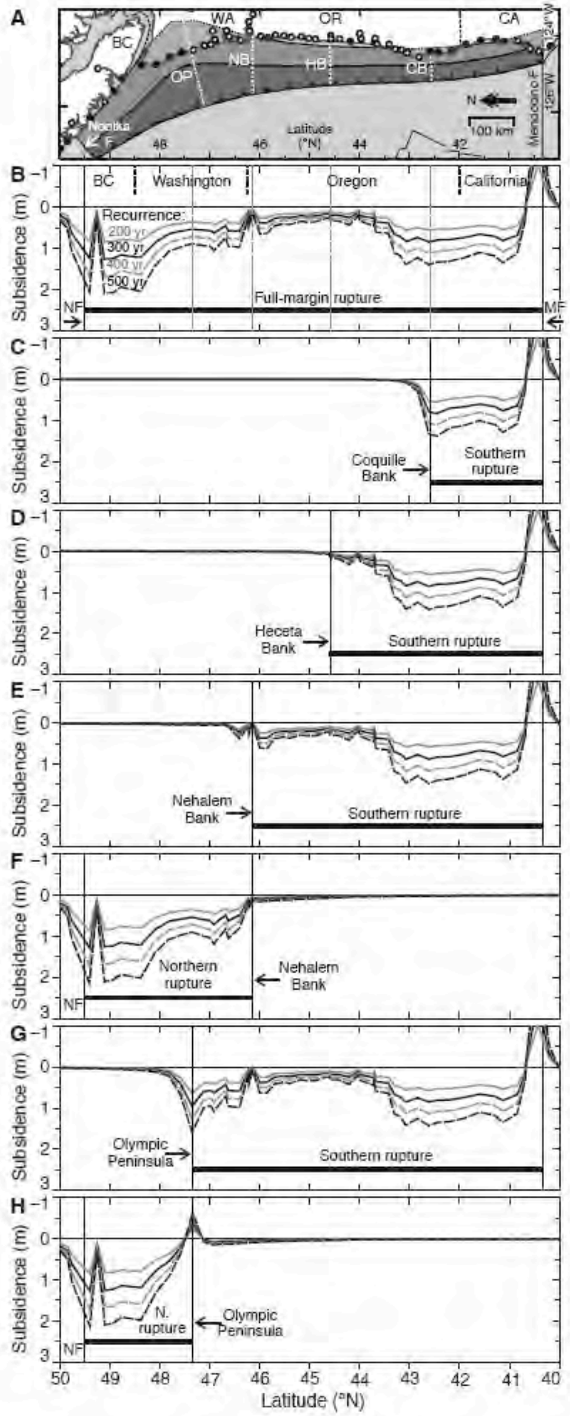
A
WA
OR
CA
BC
OP
NB
HB
CB
N
100 km
Latitude (°N)
Mendocino F
Nootka F
B
BC
Washington
Oregon
California
Recurrence:
200 yr
300 yr
400 yr
500 yr
Full-margin rupture
NF
MF
C
Coquille Bank
Southern rupture
D
Heceta Bank
Southern rupture
E
Nehalem Bank
Southern rupture
F
Northern rupture
Nehalem Bank
NF
G
Olympic Peninsula
Southern rupture
H
N. rupture
Olympic Peninsula
NF
Subsidence (m)
Latitude (°N)

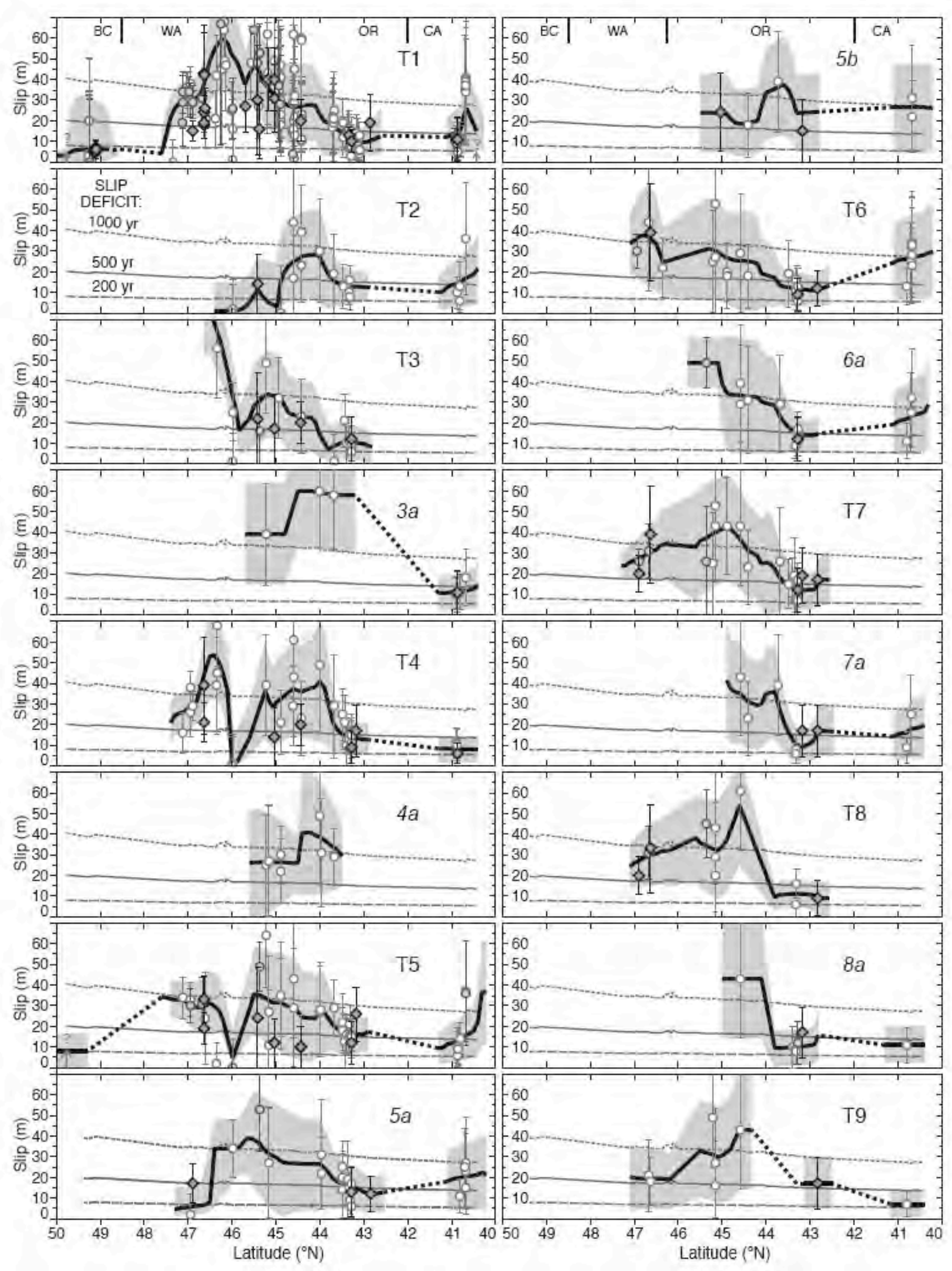

BC
WA
OR
CA
T1
5b
SLIP
DEFICIT:
1000 yr
500 yr
200 yr
T2
T6
T3
6a
3a
T7
T4
7a
4a
T8
T5
8a
5a
T9
Slip (m)
Latitude (°N)

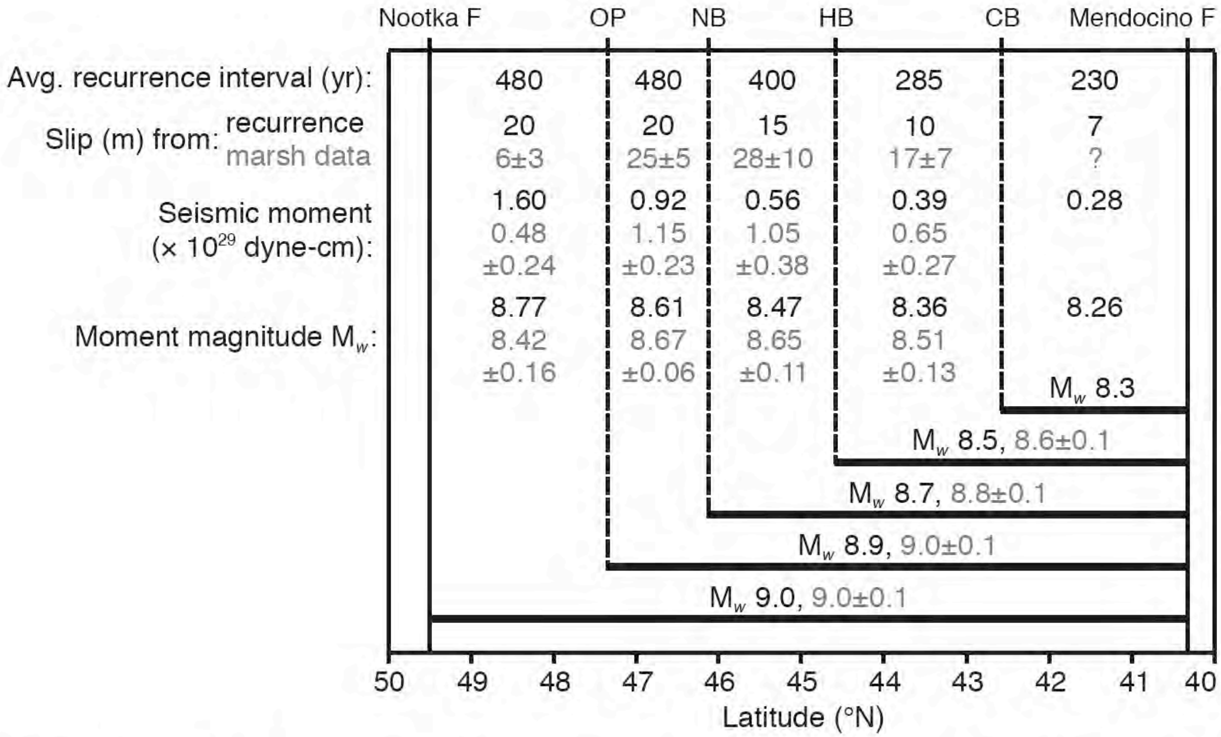

Figure 10. Moment magnitude values estimated for full-margin and segmented ruptures of the Cascadia megathrust. Seismic moment is estimated using the equation $M_o = \mu As$ (Hanks and Kanamori, 1979), where μ, the shear modulus, is taken to be 3.0×10^{11} dyne-cm (a typical value for crustal rocks; Turcotte and Schubert, 2002), *A* is the rupture area, and *s* is the magnitude of slip. Rupture widths are approximated downdip by the width of the full-rupture zone and half the width of the transition zone, and rupture lengths are measured between the Nootka and Mendocino faults and the various segment boundaries shown in Figure 7. Slip values are approximated for each segment of the margin, (1) from the expected slip related to average recurrence intervals over the past 6500 yr (black text), and (2) from the best fit to the average marsh displacements (gray text). The expected moment contribution of each segment is given for both slip approximations, along with moment magnitudes, calculated using the equation $M_w = 2/3 \log(M_o) - 10.7$ (Hanks and Kanamori, 1979). Moment magnitudes are also given for various rupture modes shown in Figure 7. Marsh data for the northernmost segment are based only on the A.D. 1700 event; a preceding interval of ~200 yr is expected to lead to an earthquake with 8 m slip, 0.64×10^{29} dyne-cm moment release, and M_w 8.50. Abbreviations: Coquille Bank (CB), Heceta Bank (HB), Nehalem Bank (NB), and the Olympic Peninsula (OP).

New aeromagnetic data reveal large strike-slip (?) faults in northern Willamette Valley, Oregon

Blakely et al 2000

GSA Bulletin pp. 1225-1233

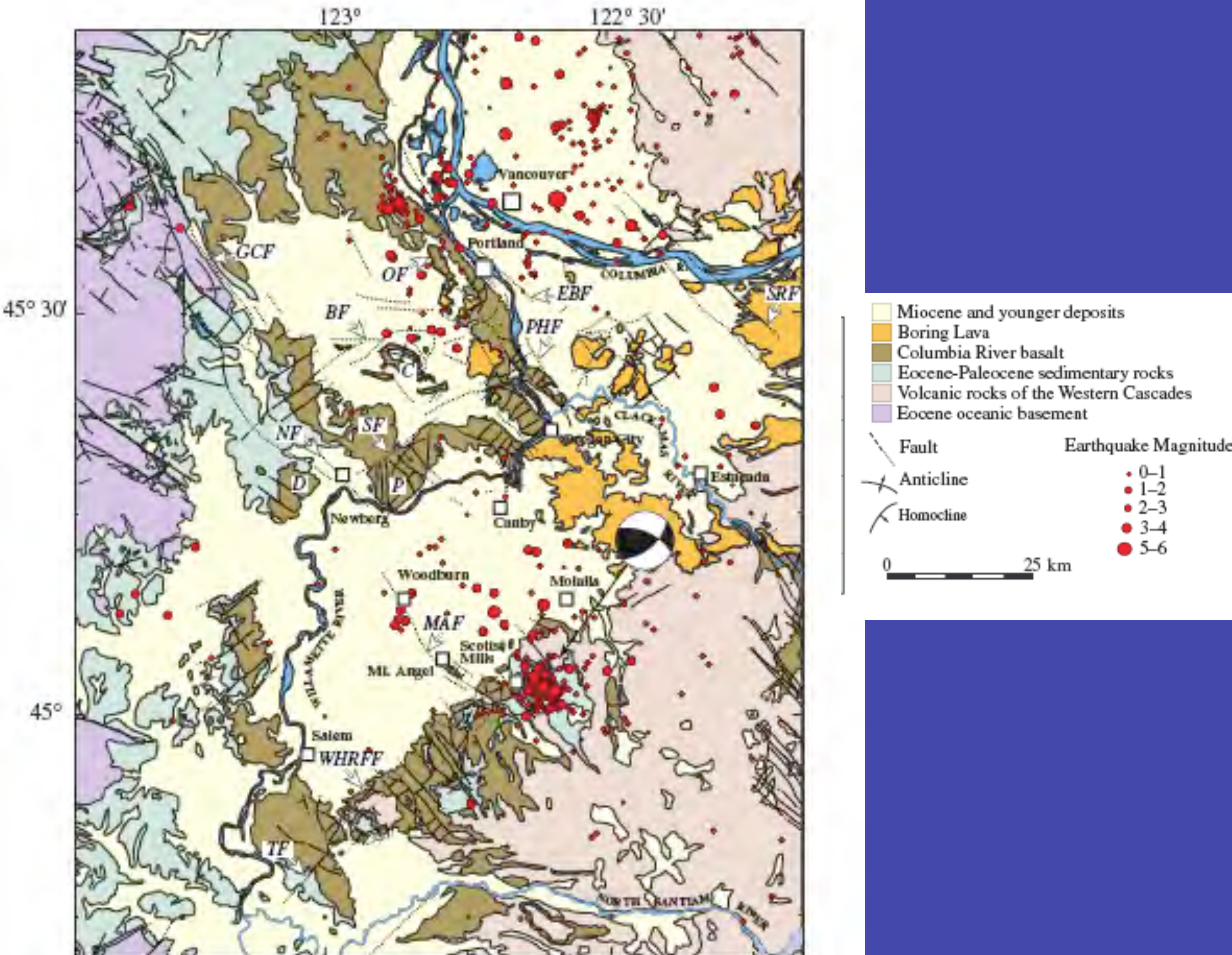

123°
122° 30'
45° 30'
45°
Vancouver
Portland
COLUMBIA
GCF
OF
EBF
BF
PHF
SRF
C
NF
SF
D
P
Newberg
Canby
Estacada
Woodburn
Molalla
MAF
Scotts Mills
Mt. Angel
Salem
WHRFF
TF
WILLAMETTE RIVER
NORTH SANTIAM RIVER
Miocene and younger deposits
Boring Lava
Columbia River basalt
Eocene-Paleocene sedimentary rocks
Volcanic rocks of the Western Cascades
Eocene oceanic basement
Fault
Anticline
Homocline
Earthquake Magnitude
0–1
1–2
2–3
3–4
5–6
0
25 km

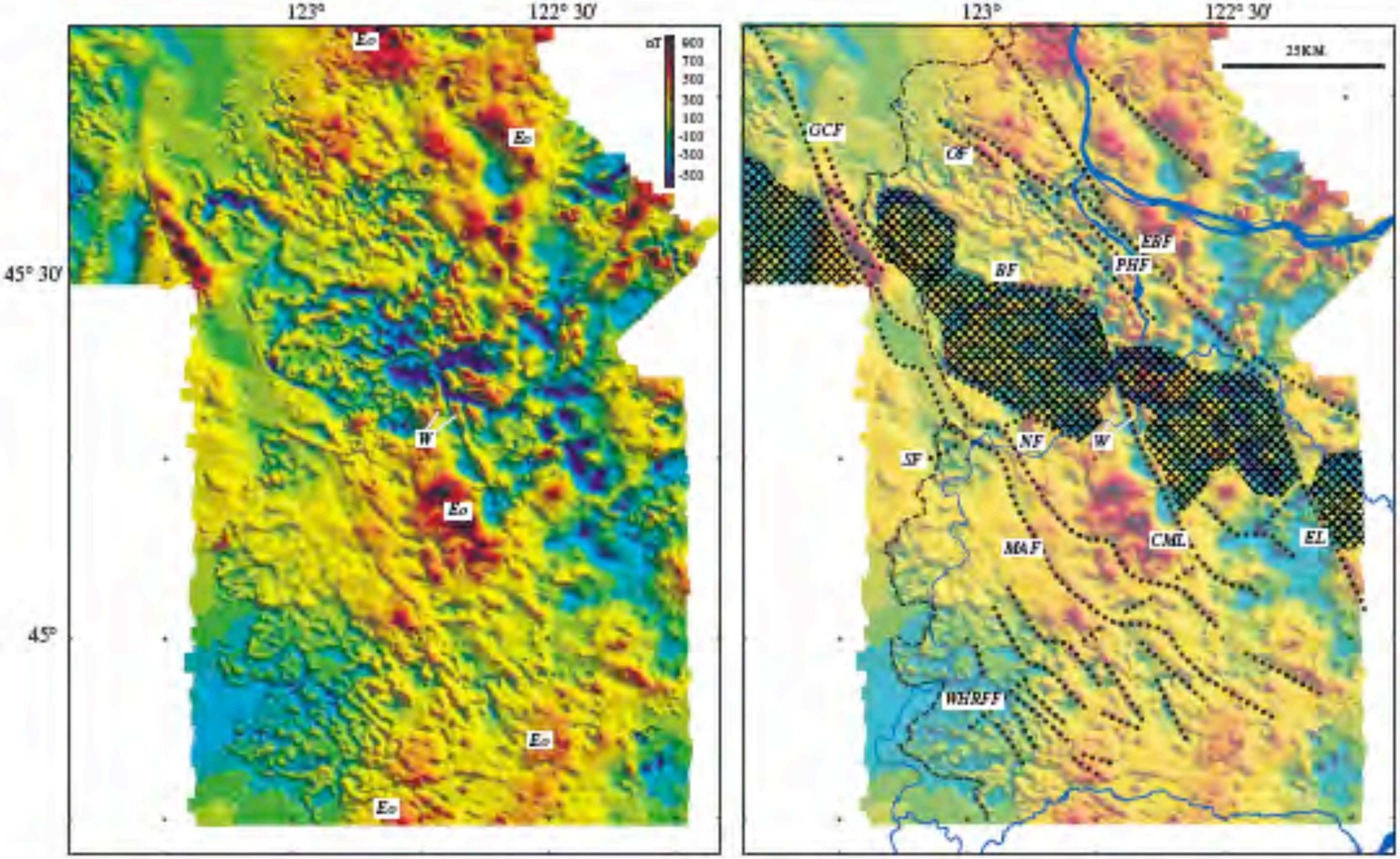

Figure 2. (A) Aeromagnetic anomalies of the northern Willamette Valley. Color scale represents intensity of crustal magnetic field, expressed in nanoteslas (nT). Eo—high-amplitude anomalies suspected of being caused by Eocene oceanic basalt basement. (B) Interpretation of aeromagnetic anomalies. Dotted lines indicate magnetic lineaments. Dashed line is western extent of Columbia River basalt flows. Cross-hachured areas are magnetic lows discussed in text. CML—Canby-Molalla lineament; EL—Estacada lineament; W—anomaly across Willamette River dextrally offset along Canby-Molalla lineament. See Figure 1 caption for other abbreviations.

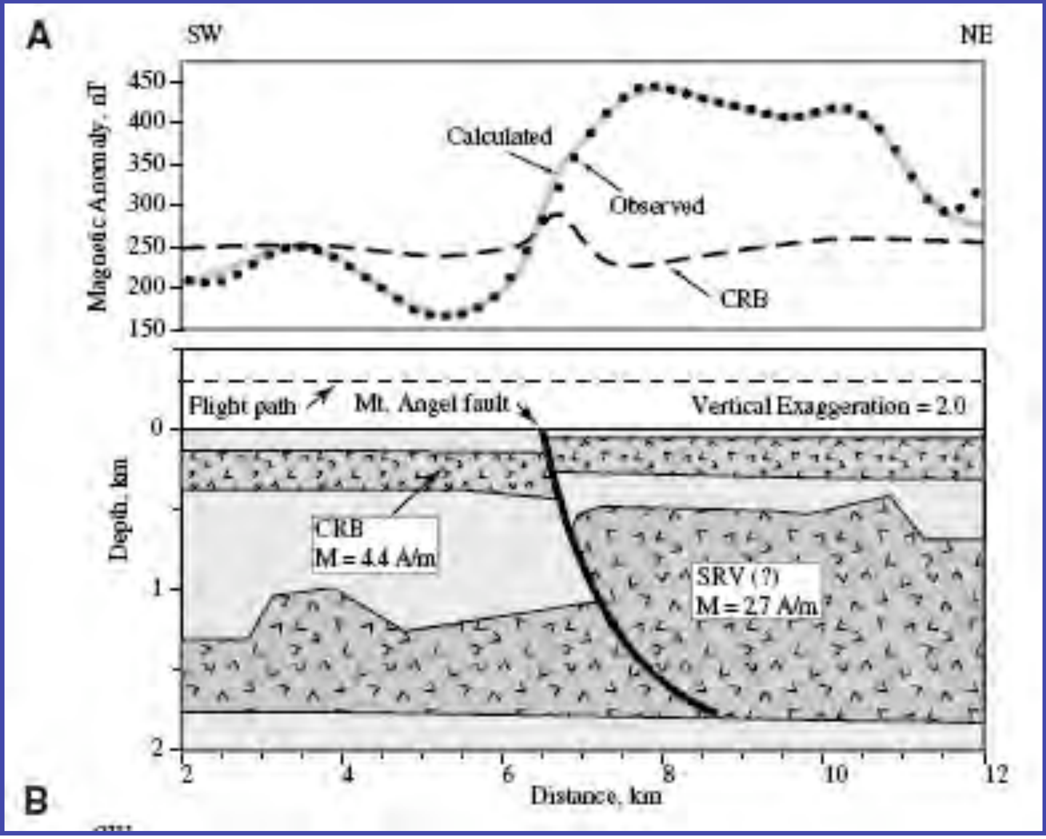
A
SW
NE
Magnetic Anomaly, nT
Calculated
Observed
CRB
Flight path
Mt. Angel fault
Vertical Exaggeration = 2.0
Depth, km
CRB
M = 4.4 A/m
SRV (?)
M = 2.7 A/m
Distance, km

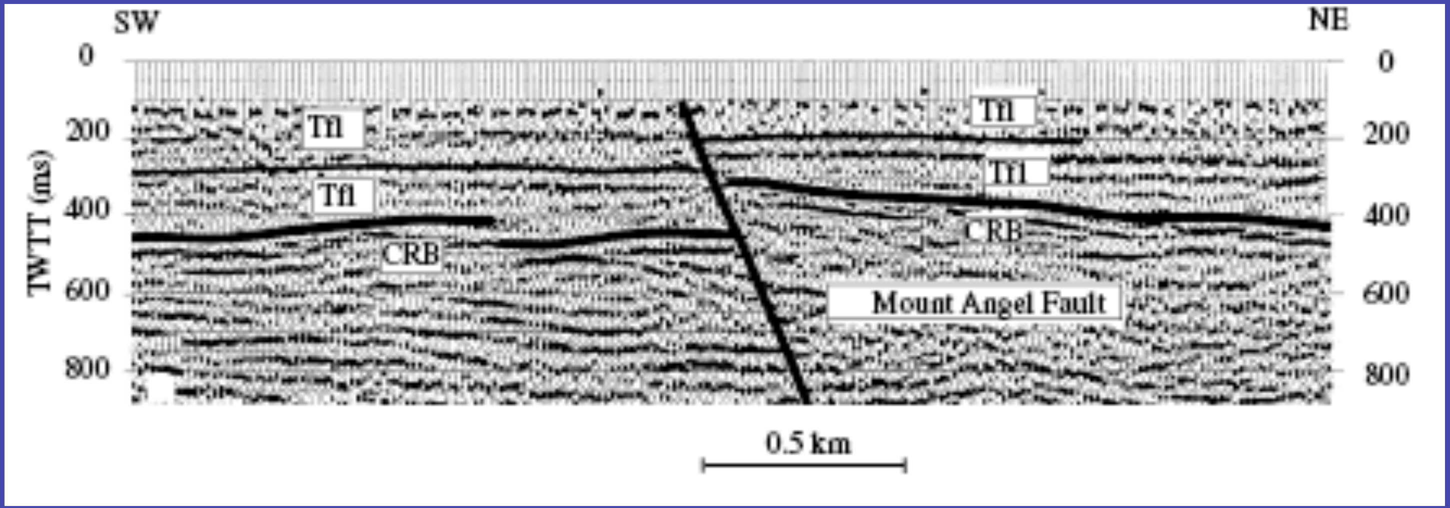
B
SW
NE
TWTT (ms)
Tfl
Tfl
CRB
Tfl
Tfl
CRB
Mount Angel Fault
0.5 km

Forearc migration in Cascadia and its neotectonic significance

Wells et al 1998

Geology pp 659-652.

“The Big Picture”

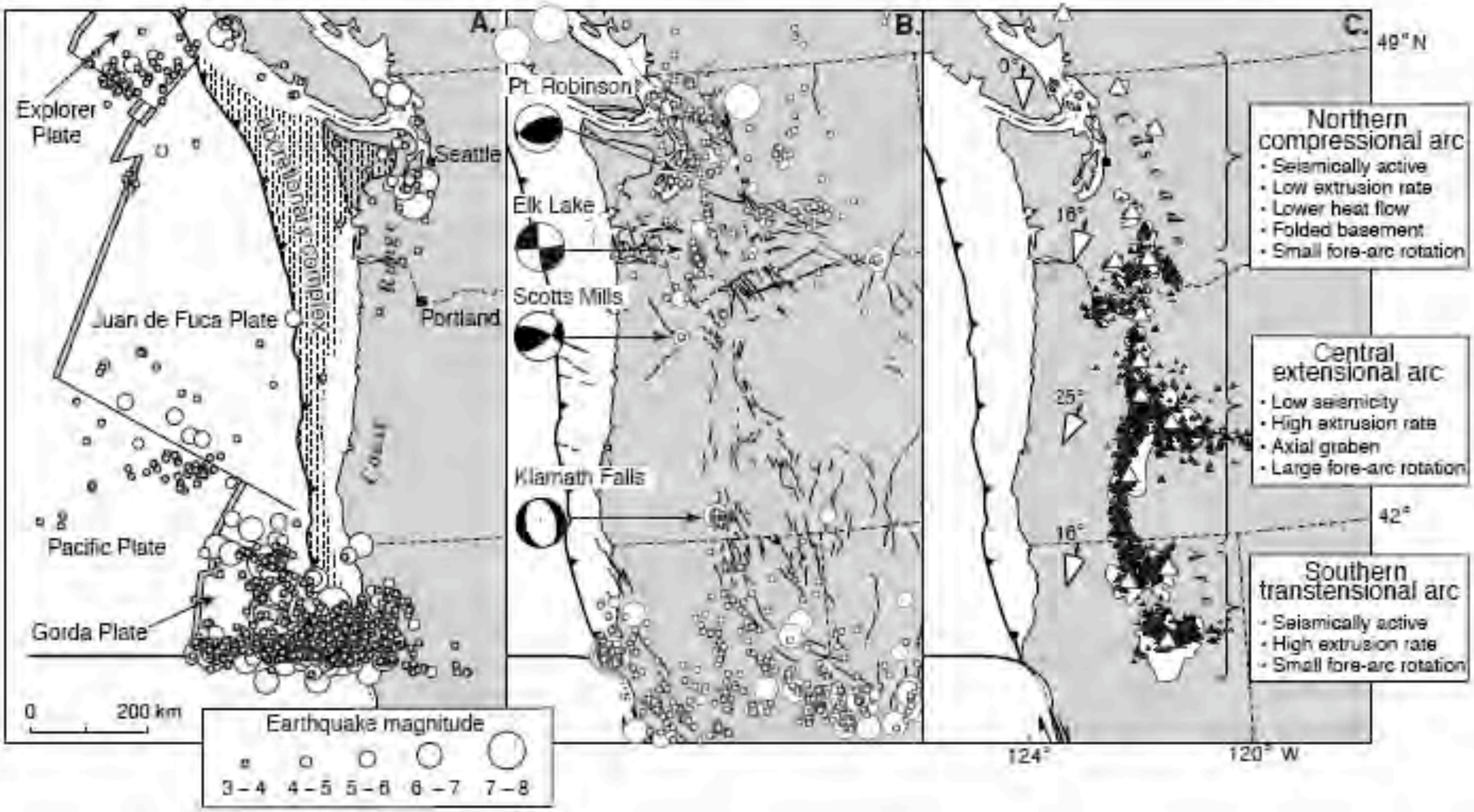

Figure 2. Cascadia earthquakes, faults, volcanoes, and fore-arc rotation (see text). A: Lower plate seismicity. B: Upper plate seismicity, recent focal mechanisms ($M_w > 5$), and late Cenozoic faults. C: Quaternary arc volcanism—white; major volcanoes—open triangles; post–5 Ma volcanic vents—filled triangles; fore-arc rotations with uncertainties—arrows (Pezzopane and Weldon, 1993; Sherrod and Smith, 1990; Guffanti and Weaver, 1988; Wells, 1990; Wiley et al., 1993; Madin et al., 1993).

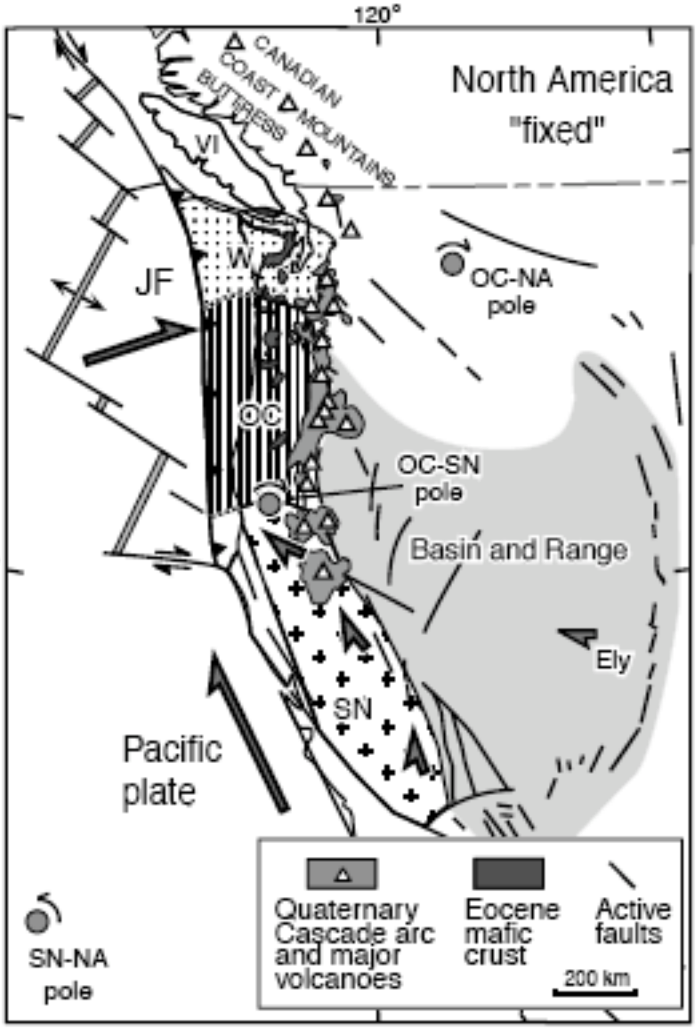

Figure 1. Tectonic setting of Cascadia. Juan de Fuca plate (JF) is subducting (barbed fault) beneath North America. Migrating Cascadia fore-arc terrane divided into Washington (W), Oregon Coastal (OC), and Sierra Nevada blocks (SN). "Instantaneous" Euler rotation poles shown for SN relative to North America (NA), OC-SN, and OC-NA. VI—Vancouver Island.

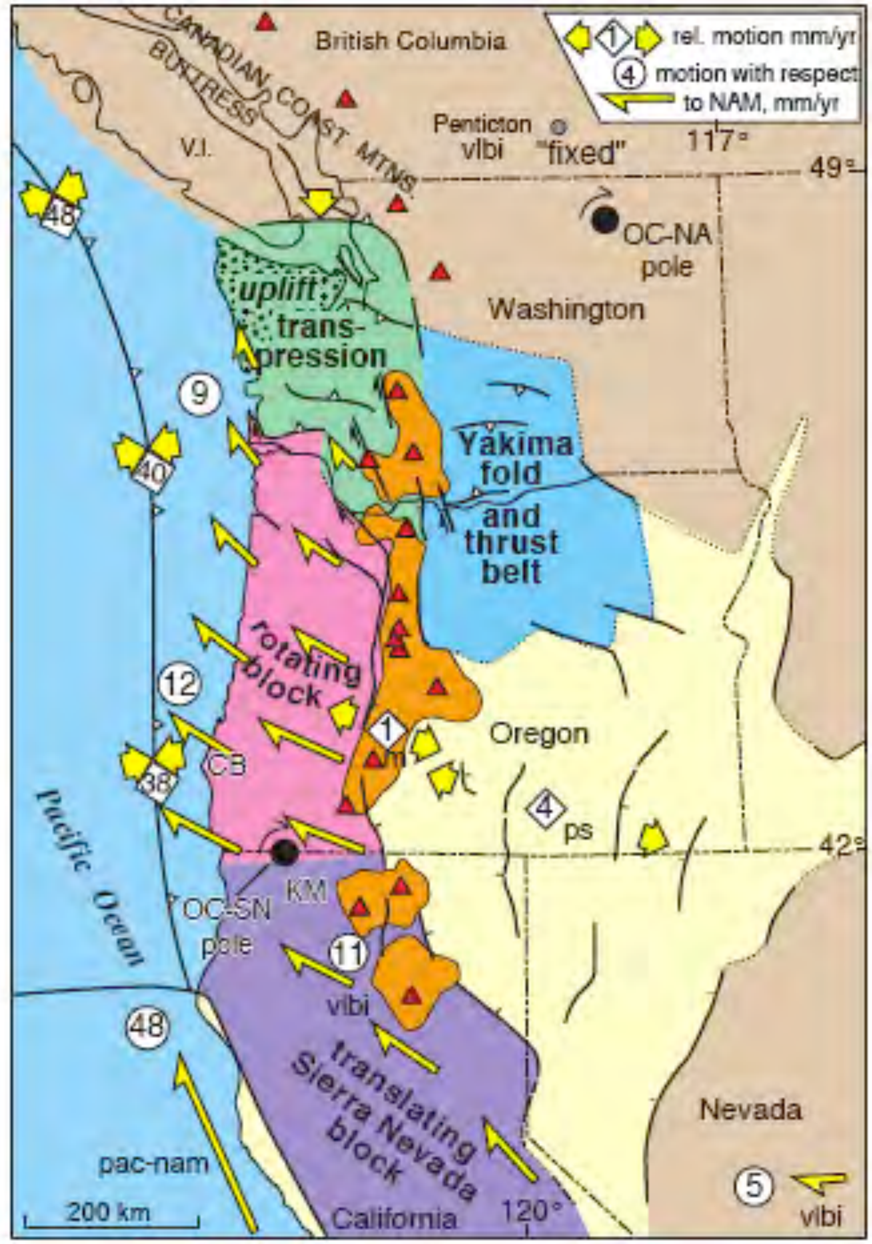

Earthquake Hazard Maps
Portland, OR
1. Portland Hills 6.8
2. Subduction Zone 9.0

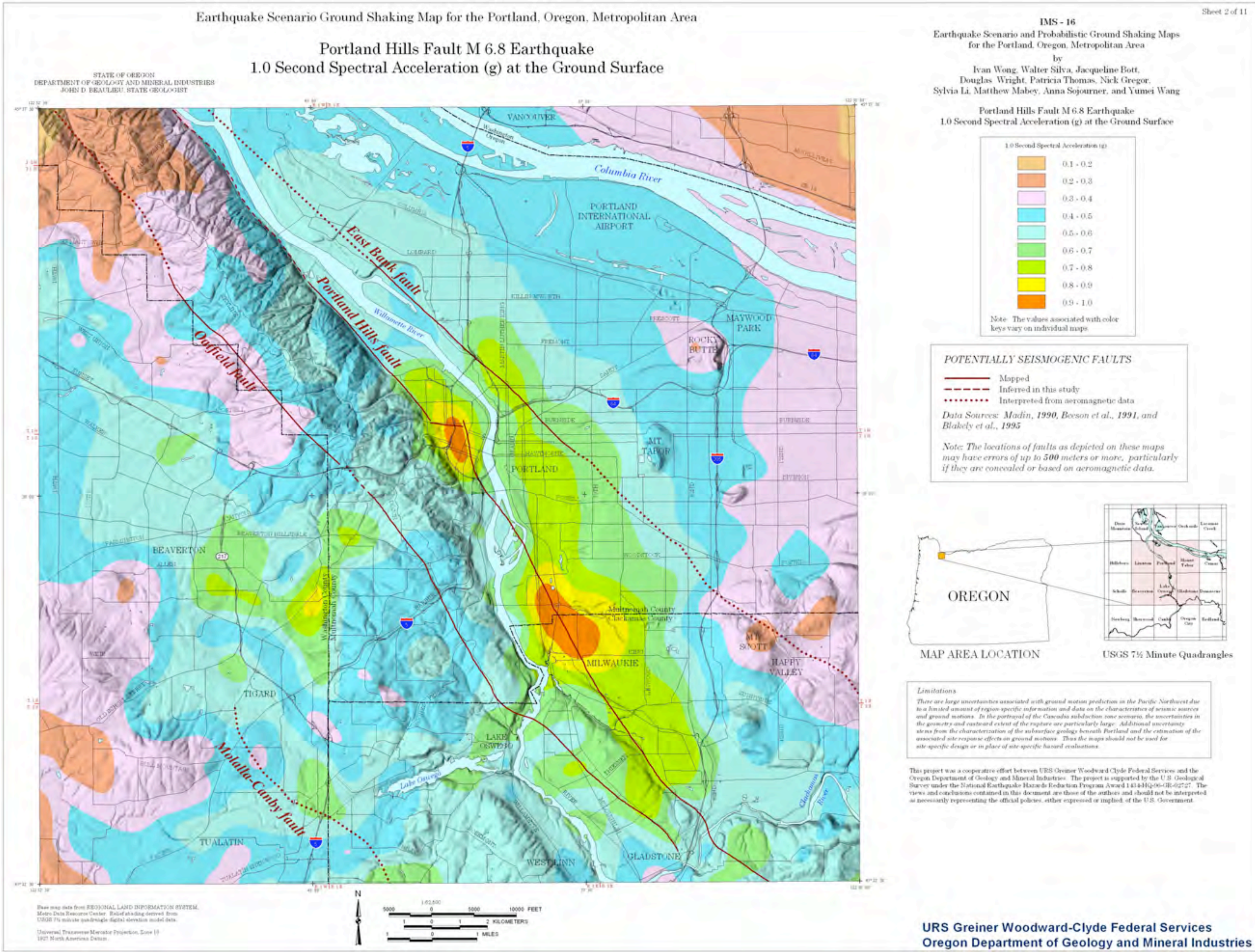

Shaking associated with a M 6.8 earthquake in Portland Hills

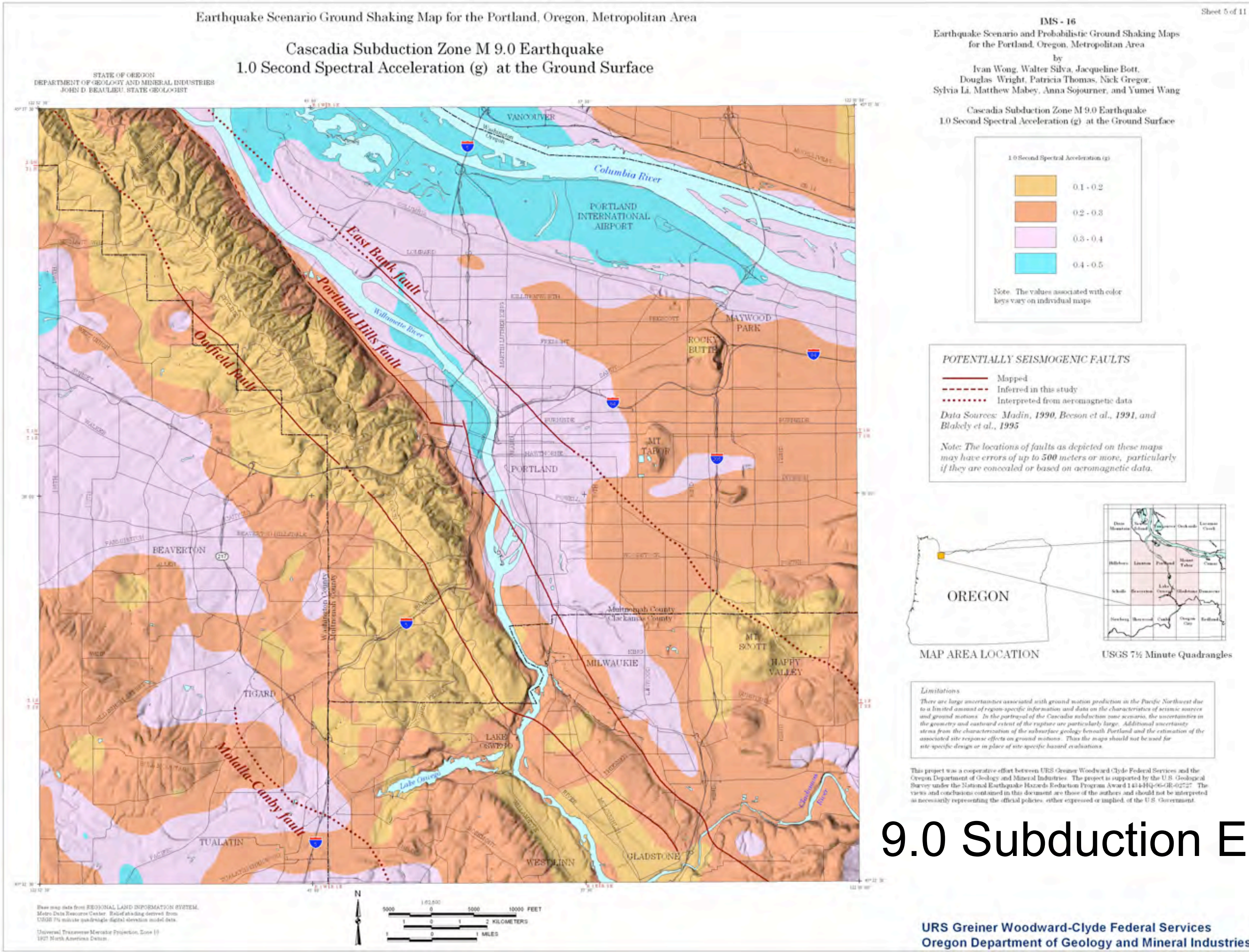

9.0 Subduction EQ

NB Shaking is one-half that of a local 6.8 earthquake